METHODS OF CALCULATIONS

In this section, a very brief description of computational chemistry methods is presented to provide an overview of the quantum mechanical technique utilized in this thesis. An in-depth detail of the computational methods can be found in the relevant text books. The Density functional theory (DFT) and the resolution of the identity (RI) are selected as the method used throughout this thesis.

Density functional theory (DFT) is one of the most widely used techniques for computational chemistry nowadays. Its advantages include less demanding computational effort, less computational time and better agreement with the experimental values than that of the Hartree-Fock procedures.

The central focus of DFT is the electron density, ρ, rather than the wavefunction ψ. The energy part of the molecules is a function of the electron density, $E[\rho]$ and the electron density is itself a function of position, ρ(r). The exact ground-state energy of an n-electrons molecule is

$$E[\rho] = T[\rho] + E_{ne}[\rho] + E_{ee}[\rho] + E_{XC}[\rho] \tag{1}$$

where $T[\rho]$ is the total electron kinetic energy, $E_{ne}[\rho]$ the electron-nucleus potential energy, $E_{ee}[\rho]$ the electron-electron potential energy, and $E_{XC}[\rho]$ the *exchange-correlation energy*, which takes into account all the effects due to all interactions among electrons in the system. The orbitals used to construct the electron density from

$$\rho(r) = \sum_{i=1}^{n} |\psi_i(r)|^2 \tag{2}$$

are calculated from the *Kohn-Sham equations*, which are found by applying the variational principle to the electron energy, and are like the Hartree-Fock equations except for a term V_{XC}, which is called the exchange-correlation potential:

$$\left\{-\frac{\hbar^2}{2m_e}\nabla_1^2-\sum_{j=1}^{N}\frac{Z_j e^2}{4\pi\varepsilon_0 r_{j1}}+\int\frac{\rho(r_2)e^2}{4\pi\varepsilon_0 r_{12}}dr_2+V_{XC}(r_1)\right\}\psi_i(r_1)=\varepsilon_i\psi_i(r_1) \qquad (3)$$

The exchange-correlation potential is the 'functional derivative' of the exchange-correlation energy:

$$V_{XC}[\rho]=\frac{\delta E_{XC}}{\delta\rho} \qquad (4)$$

The Kohn-Sham equations are solved iteratively and self-consistently. First the electron density is guessed. For this step it is common to use a superposition of atomic electron densities. Then the exchange-correlation potential is calculated by assuming an approximate form of the dependence of the exchange-correlation energy on the electron density and evaluating the functional derivative in equation (4).

The major problem of DFT is that an exact term for $E_{XC}[\rho]$ is not known and approximate functionals must be used. Thus, many types of functionals are available; the simplest approximation is the *local-density approximation (LDA)*, which is dependent only on the electron density. The *Generalized Gradient Approximation (GGA)* functionals include the gradient of the electron density as well as the electron density. The *Hybrid functional* has also been proposed. The B3LYP functional is one such functional that is the most widely used nowadays. DFT can be implemented either with an atom-centered localized basis set or with a plane-wave basis set. Such basis sets are also used in this thesis works as will be stated in the "Models and Methodologies" section.

The basic approach to all these methods is the factorization of the four-center integral into two parts:

$$(ij|kl) = \sum_{\gamma}^{N} L_{ij\gamma} R_{\gamma kl} \tag{5}$$

The factorization is beneficial for any Coulomb interaction summation. The cost is now O(n^3)., as opposed to the O(n^4). for traditional integral evaluation. Unfortunately, this factorization does not formally reduce the scaling of an exchange interaction summation. The time to compute the quantities used in the Coulomb or exchange interaction summations will vary but the cost of the summation remains O(n^4) for the exchange term.

In the RI approximation the reduction is formally introduced by inserting a resolution of the identity into the two-electron integrals:

$$(ij|kl) \approx \sum_{t} (ijt)(t|kl) \tag{6}$$

Unless the auxiliary basis |t) spans the whole space of products |ij), this expansion introduces an error showed that by inserting the resolution of the identity more than once and minimizing different properties of the residual function.

Three different three-center approximations for the four-center two-electron integrals result:

$$(ij|kl) = \sum_{tuvw} (ijt)\ S_{tu}^{-1} V_{uv} S_{vw}^{-1} (klw) \tag{7}$$

$$(ij|kl) = \sum_{tu} (ijt)\ S_{tu}^{-1} (kl|u) \tag{8}$$

$$(ij|kl) = \sum_{tu} (ij|t) V_{tu}^{-1} (kl|u) \tag{9}$$

Depending on the term between the three-center integrals, they are named SVS-, S-, and V-approximation, which correspond to Eqs. (7), (8), and (9), respectively. The two-center quantities are the overlap (S_{tu} = (tu)) and electron repulsion (V_{tu} = ($t|u$)) integrals using the auxiliary functions or the RI fitting basis. Preliminary comparisons show that self-consistent field (SCF) energies and energy differences obtained with the V-approximation are on average more accurate by two orders of magnitude than the others.

This is not surprising, as the V-approximation is used extensively in DFT theory to approximate the Coulomb contribution. This in principle also holds for the exchange contribution, but as the sign of Coulomb and exchange part are different, the sum is not variational. In addition, the optimal basis for the two contributions is different, and using the same basis takes away the "best approximation" argument. Nevertheless it gives further indication that the V-approximation is the more natural one to use.

Besides the "traditional"' use in DFT, the RI approximation has been implemented for SCF, multi-configuration self-consistent field (MCSCF), MP2, and coupled cluster singles and double (CCSD) with and without perturbative triples. An exchange-type sum does not reduce the O(n^4) scaling of the calculation, but this does not necessarily mean that a reduction of work cannot be accomplished. In a disk-based implementation, the storage as well as the I/O requirement scale only with the third power of the number of basis functions, O(n^3). Also, in a fully direct implementation the integral calculation, normally the most time-consuming step, would not only take advantage of the cheaper three-center integrals, but also only scale with O(n^3). The O(n^4) part consists only of matrix multiplications, which are in most cases computationally much less expensive than integral calculations. In addition, linear algebra operations are a very general problem, so one can expect that efficient implementations are available for most computer architectures.

In the implementation, the matrix V^{1} in Eq. (9) is not stored, but contracted into the three-center integrals. The integrals are transformed with $V^{1/2}$ and the transformed integrals ($ij|v$) are used in the requisite summations.

$$(ij|kl) = \sum_{stu} (ij|s)\ V_{st}^{-1/2} V_{tu}^{-1/2} (u|kl) \tag{10}$$

$$= \sum_{v} (ij|v)\,(v|kl) \tag{11}$$

The expansion or fitting basis sets developed for the DGauss and DeMon density functional programs that are widely used for DFT calculations are based on the same theme. A mostly (all except the highest exponent) even-tempered set, starting with double the lowest exponent of the atomic orbital basis set, is constructed with as many exponents as possible shared between the different angular momenta to simplify integral calculation. Although the small number of functions, and especially the lack of functions with high angular momentum (even for second-row atoms and transition metals they only go up to d functions), seems rather limiting, the large number of successful applications seems to indicate that chemically reasonable results can be obtained with them.

One significant systematic optimization of a basis set for use as an RI expansion basis is the work on an expansion basis for use in DFT calculations. They require the exponents of their expansion basis to fulfill a dependency similar to the definition of an even-tempered basis and optimize η_0, β and γ to maximize the Coulomb energy, using its variational property.

$$\eta_{i+1} = \eta_i \beta \left(1 + \gamma \frac{i^2}{(n+1)^2} \right) \tag{12}$$

The number of functions and highest angular momentum are chosen to fulfill an accuracy criterion for the charge density with a minimal number of expansion functions.

A more thorough investigation of this problem is clearly necessary. It may turn out that basis sets have to have different properties for different methods, depending on if Coulomb or exchange interaction contributions are more important, or if the core or the valence electrons have to be described more accurately.

The main use of the DOS plots is to provide a pictorial representation of MO compositions and their contributions to chemical bonding through the overlap population density-of-states plots which the total density of states (TDOS) at energy *E* is written as

$$TDOS(E) = \sum_i \delta(E - \varepsilon_i) \tag{13}$$

Where the summation index *i* goes over all one-electron energy levels. Thus, the integral of *TDOS*(*E*) over an energy interval (E_1 to E_2) gives the number of one-electron states in that energy interval.

The DOS calculation in this work, the δ-function can be substituted by Lorentzians, Gaussians, or pseudo-Voigt functions *F*:

$$TDOS(E) = \sum_i F(E - \varepsilon_i) \tag{14}$$

In order to find out how much a given fragment *A* (an orbital, an atom, a group of orbitals, or a group of atoms) contributes to one-electron levels at certain energies, one may weigh a one-electron level with the fragment character, $C_{A,i}$. These fragment characters are determined by mean of MPA or SCPA. Thus, for the partial density of states, one gets:

$$PDOS_A(E) = \sum_i C_{A,i} F(E - \varepsilon_i) \tag{15}$$

A sum $PDOS_A(E)$ for all fragments gives $TDOS(E)$:

$$TDOS(E) = \sum_A PDOS_A(E) \tag{16}$$

The overlap population density-of-states for fragments A and B, is

$$OPDOS_{AB}(E) = \sum_i OP_{AB,i} F(E - \varepsilon_i) \tag{17}$$

The integration of the $OPDOS_{AB}(E)$ function over all populated levels gives the total overlap population TOP_{AB} between fragments A and B:

$$TOP_{AB} = \int_{-\infty}^{E_F} OPDOS_{AB}(E) dE \tag{18}$$

Positive $OPDOS_{AB}(E)$ regions represent energy regions where *A*-*B* bonding levels are located. Thus, the *OPDOS* functions enable one to ascertain the bonding characteristics of electronic levels in a given energy range with respect to any pair of molecular fragments. Since calculations of the *OPDOS* functions require the overlap populations $OP_{AB,i}$, the *OPDOS* plots are only calculated for non-ZDO calculations with MPA as a method for electron population analysis.

The model of SWCNT(5,5) consists of 90 carbon atoms. At each end of the model, 10 terminated H atoms were added to preserve the sp^2 hybridization structure of carbon atoms at the edge of the tube, yielding the model, namely, a $C_{90}H_{20}$. Fig 6 shows the model of single BN doped on the armchair SWCNT which two <adjacent> carbon atoms of the SWCNT were replaced by B and N atoms at the most stable position reported in literature, giving the model of BN-doped SWCNT namely $BNC_{88}H_{20}$. In order to express the functionalization of BN-doped SWCNT system, effects of nitrogen nucleophiles (N-nucleophiles) to the BN-doped SWCNT were explored. Different types of N-nucleophiles (see Fig. 7), *i.e.*, ammonia, arginine, chitosan, guanidine, imidazole, m-nitroaniline and pyridine, were selected to study. We noted that all N-nucleophiles are named as *R-group* throughout the article. *R*-

group (Amine derivative N nucleophilic groups) was interacted directly to B atom of the BN-doped SWCNT due to an electron acceptor behavior of B atom.

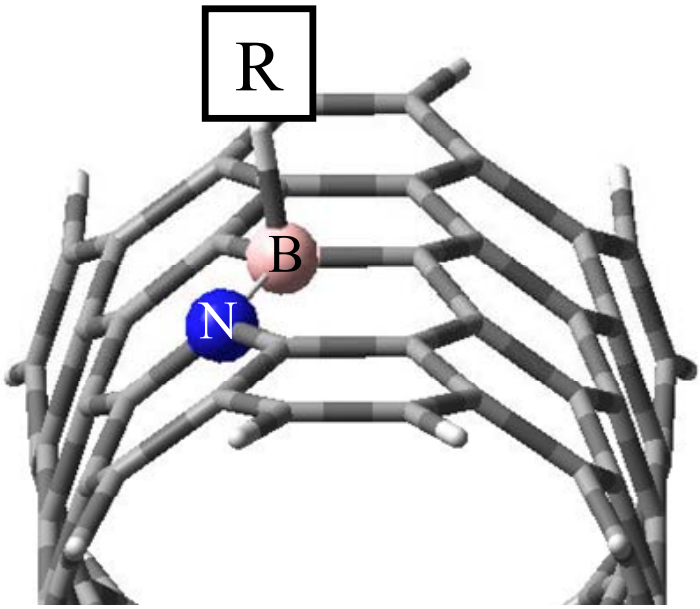

Figure 6 Position of R-group functionalization on side-wall (5,5) SWCNT

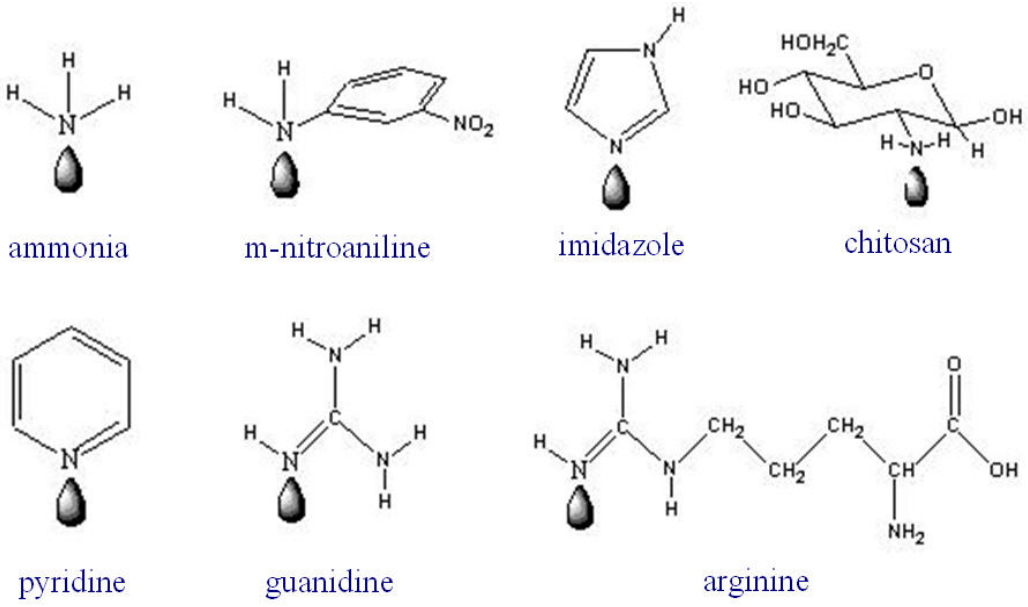

Figure 7 Structure of Nitrogen nucleophiles

Full geometry optimization of such systems have been carried out by means of density functional theory (DFT) using the PBE exchange-correlation functional implemented in TURBOMOLE code. The standard split-valence polarization SV(P) (double-ζ with polarization) basis sets with (7s4p1d)/[3s2p1d] contraction were used for all atoms in the system. Initially, we reported the functionalization of BN-doped SWCNT with N-nucleophiles in terms of binding energy and bonding geometry according to the position that the interaction takes place (see Fig. 8). The binding energies for such systems were calculated from $E_b = E_{(BN\text{-}SWCNT)} + E_{(R\text{-}group)} - E_{(BN\text{-}SWCNT/R\text{-}group)}$, where $E_{(BN\text{-}SWCNT)}$, $E_{(R\text{-}group)}$ and $E_{(BN\text{-}SWCNT/R\text{-}group)}$ are the total energies of the BN-doped SWNCT, of the nitrogen nucleophilic molecule and the complex of BN-doped SWCNT and the nitrogen nucleophilic molecule, respectively. The "*pyramidalization angle*", thus, was intuitively discussed to verify alteration in pyramidalization and hybridization ($sp^2 \rightarrow sp^3$) undergone during the chemical transformation. The *pyramidalization angle* is defined as $\theta_P = (\theta_{\sigma\pi} - 90)°$, where $\theta_{\sigma\pi}$ is the angle between the π-orbital axis vector and the three σ-bonds at a conjugated carbon atom. The θ_P suggests the sp^2 or sp^3 hybridizations when the θ_P is 0° or 19.47°, respectively. Additionally, we also reported energy gap between the HOMO and LUMO states to elucidate the effect of BN-doped to SWCNT as well as *R-group* to BN-doped SWCNT.

Finally, to gain insight into the electronic properties, we have done the electronic population analysis calculations, e.g, charge transfer (NPA analysis), DOS and atomic orbital. Such electronic properties were performed by the single point calculations using DFT-PBE and Ahlrichs pVDZ basis set as available in Gaussian 03 package. The DOS plots were convoluted by the AOMix program with the coefficient.

Fullerene (C_{60}) and BN-doped fullerene ($C_{58}BN$) were selected as reference systems as illustrated in Fig 8. As for the BN-doped fullerene, the C-C bond connecting two hexagonal structures were substituted by BN heteroatoms since it has been reported to be the most stable structure among their isomers [10-12]. Three types of heterocyclic compounds, namely, 2,6-Naphyridine ($C_8H_6N_2$, **1**), 3,8-Phenanthroline

($C_{12}H_8N_2$, **2**) and 2,6-Diazaantracene ($C_{12}H_8N_2$, **3**) are selected to study the modified interfullerene electronic conductivity (see Fig 8c-e). Such bridging compounds were interacted directly to the 'Boron atom' in the $C_{58}BN$ structure due to its high electron accepter efficiency. Likewise, two $C_{58}BN$ active centers were connected together by heterocyclic compounds by which interconnected at Boron positions of each $C_{58}BN$ ball.

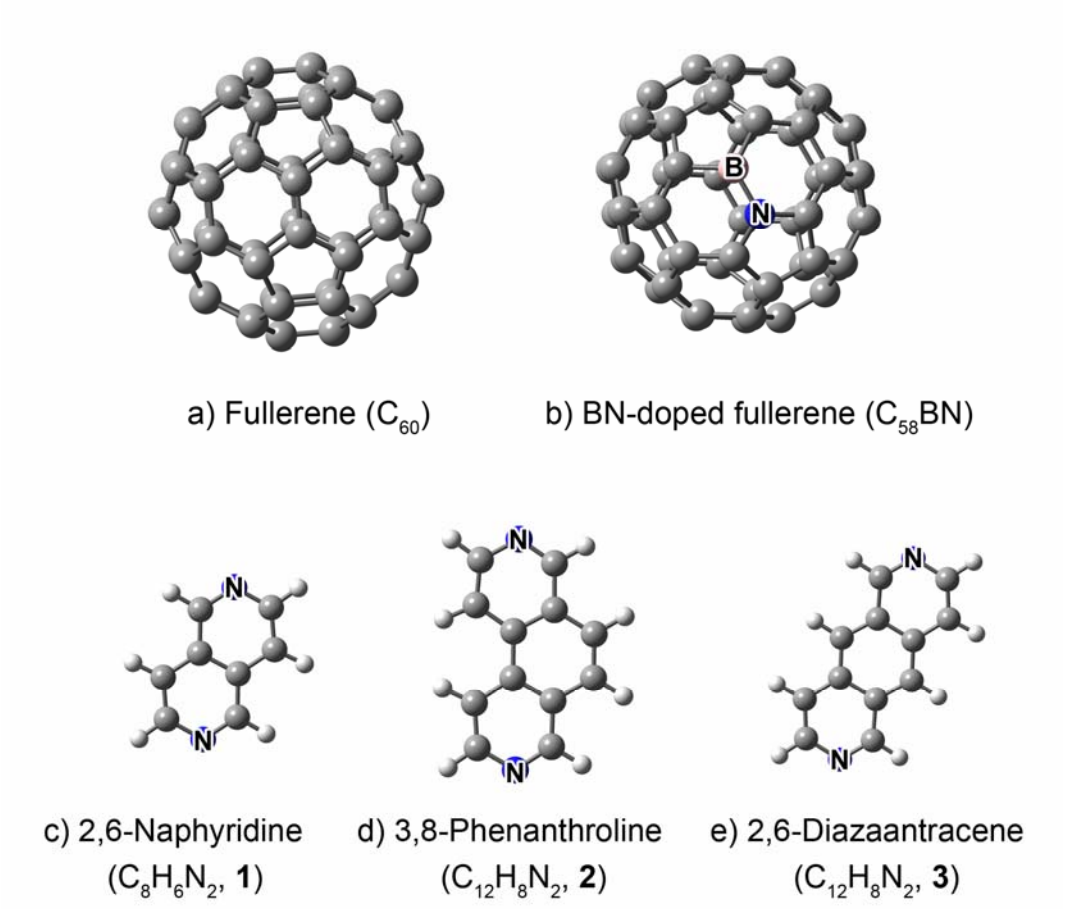

Figure 8 Illustrations of a) Fullerene (C_{60}), b) BN-doped fullerene ($C_{58}BN$), c) 2,6-Naphyridine ($C_8H_6N_2$, **1**), d) 3,8-Phenanthroline ($C_{12}H_8N_2$, **2**) and e) 2,6-Diazaantracene ($C_{12}H_8N_2$, **3**) structures.

Full geometry optimization of such systems have been carried out by means of density functional theory (DFT) using the PBE exchange-correlation functional implemented in TURBOMOLE code. The standard split-valence polarization SV(P) (double-ζ with polarization) basis sets with (7s4p1d)/[3s2p1d] contraction were used for all atoms in the system. We noted here that we neglect the underestimation of energy gaps obtained from PBE calculations since we are mainly interested in the trend observed for the electronic conductivity improvements of the connection of fullerene dimer by the spacer linkage heterocyclic compounds. We also investigated some selected systems using B3LYP/6-31G* level of theory and found that the relative energy gap alterations due to the effects of either BN doped into fullerene or the spacer linkage heterocyclic compounds are in the same order as reported in our PBE calculations (B3LYP/6-31G*: Relative energy gap reduction of $C_{58}BN$, $C_{58}BN$/**1**, $C_{58}BN$/**2** and $C_{58}BN$/**3**, compared to C_{60}, are 0.22, 1.01, 0.82 and 1.28, respectively).

We calculated the energy gaps between HOMO (highest occupied molecular orbital) and LUMO (lowest unoccupied molecular orbital) to evaluate the electronic conductivity of bisfullerene when the heterocyclic compounds are taken into account as the spacer linkages. Moreover, the HOMO and LUMO contour plots for selected systems are also demonstrated to clarify how electronic properties of systems alter as a result of bridging heterocyclic compounds.